Research article

Jeeyoon Jeong, Dasom Kim, Hyeong-Ryeol Park, Taehee Kang, Dukhyung Lee, Sunghwan Kim, Young-Mi Bahk[a] and Dai-Sik Kim*

Anomalous extinction in index-matched terahertz nanogaps

https://doi.org/10.1515/nanoph-2017-0058
Received May 22, 2017; revised July 31, 2017; accepted August 1, 2017

Abstract: Slot-type nanogaps have been widely utilized in transmission geometry because of their advantages of exclusive light funneling and exact quantification of near-field enhancement at the gap. For further application of the nanogaps in electromagnetic interactions with various target materials, complementary studies on both transmission and reflection properties of the nanogaps are necessary. Here, we observe an anomalous extinction of terahertz waves interacting with rectangular ring-shaped sub-30 nm wide gaps. Substrate works as an index matching layer for the nanogaps, leading to a stronger field enhancement and increased nonlinearity at the gap under substrate-side illumination. This effect is expressed in reflection as a larger dip at the resonance, caused by destructive interference of the diffracted field from the gap with the reflected beam from the metal. The resulting extinction at the resonance is larger than 60% of the incident power, even without any absorbing material in the whole nanogap structure. The extinction even decreases in the presence of an absorbing medium on top of the nanogaps, suggesting that transmission and reflection from nanogaps might not necessarily represent the absorption of the whole structure.

Keywords: terahertz nanogaps; reflection; field enhancement; terahertz nonlinearity; index matching.

1 Introduction

Metallic nanogaps with diverse geometries such as dipole antenna [1–4], dimers or arrays of nanoparticles [5–8], negative slots [9–13], or slits [14–18] have been widely investigated for their application potential in various optical phenomena. Among them negative slot or slit antenna structures possess the advantage of background-free exclusive electromagnetic funneling when operated in transmission geometry, and is, therefore, capable of experimentally determining the near-field enhancement at the gap [19]. Such properties are advantageous in applications where quantitative analyses are highly required, such as in nonlinear experiments [10, 20–22] or when realizing molecular absorption or scattering enhancement [23–25]. Physical origins of the observed phenomena are mostly interpreted in terms of changes in transmission spectra, while the reflection counterpart, an excellent additional source of information, is usually not considered in the transmission type nanogaps. This additional information becomes more important when the nanogaps are combined with other materials, where decrease in transmission induced by the materials cannot be unambiguously interpreted as an increase in absorption or reflection. It is, therefore, essential to first investigate the transmission and reflection behavior of the nanogaps themselves in order to study the interaction between the nanogaps and target materials.

In this study we perform transmission and reflection measurements on terahertz (THz) nanogaps to quantify the power flow at the gap. Extraordinary transmission and field enhancement of THz waves in nanogaps have been theoretically studied [26] and experimentally realized, recently at gap sizes down to 1 nm [27] and below [20]. We especially focus on the effect of illumination side, from the substrate side or the air side, for wider applications in

[a]Present address: Max Planck Institute for the Structure and Dynamics of Matter, Hamburg 22761, Germany.
***Corresponding author: Dai-Sik Kim,** Department of Physics and Astronomy and Center for Atom Scale Electromagnetism, Seoul National University, Seoul 08826, Korea, e-mail: dsk@phya.snu.ac.kr.
http://orcid.org/0000-0002-8950-1199
Jeeyoon Jeong, Dasom Kim, Taehee Kang, Dukhyung Lee, Sunghwan Kim and Young-Mi Bahk: Department of Physics and Astronomy and Center for Atom Scale Electromagnetism, Seoul National University, Seoul 08826, Korea
Hyeong-Ryeol Park: Department of Physics, Chungbuk National University, Chungbuk 28644, Korea

future research. The THz frequency is very well suited for this experiment as most noble metals in this regime have extremely high electric permittivity [28, 29], shutting off direct transmissions through the unpatterned metal film and thereby enabling exclusive electromagnetic energy funneling through the gap. Also, relatively higher refractive indices of common substrates (2.1 ~ 3.4) in the THz frequency range compared to those used in visible (1.3 ~ 1.8) regime help increase the contrast for the possible substrate effects. In this experiment, nanogap samples are fabricated on top of silicon substrates with a refractive index of n = 3.2.

2 Results and discussion

A THz time-domain spectroscopy is constructed for simultaneous measurements of transmission and reflection (Figure 1A). Single-cycle THz pulses from biased GaAs emitter are weakly focused with off-axis parabolic mirrors (NA = 0.25) and illuminate the nanogap samples, either on the air-side or on the substrate-side direction. Transmitted and reflected THz waves are collected and detected with electro-optic sampling. Some 200 nm-thick Au nanogap samples are fabricated using atomic layer lithography technique [27] with the gaps rectangular ring-shaped with 10, 20, and 30 nm widths, and lengths of long and short sides of the rectangle being 80 and 20 μm, respectively (Figure 1B). Incident polarization is perpendicular to the long side of the rectangular ring such that the fundamental mode of the coaxial rectangular waveguide can be excited. As only one polarization is measured, each of the rectangle effectively behaves as a couple of linear slot antennas of 100 μm length, where field from only the middle 80 μm region contributes to the measured transmittance (see Supplementary material). Bare silicon substrate is used as a reference for transmission measurements, while unpatterned, 200 nm-thick Au film is used for reflection measurements.

Figure 2 shows the normalized transmission data for the nanogap samples. The overall transmission does not change regardless of the illumination side, as is the case for simple stacks of dielectric layers (Figure 2A). This, however, means that local transmission through the nanogap layer is larger for substrate-side illumination, because transmission coefficients for entering the substrate are smaller than that for exiting the substrate by a factor of n (Figure 2C). As far-field transmitted amplitude through the gap is directly proportional to the near-field enhancement via Kirchhoff integral formalism (see Supplementary material), this indicates that the near-field enhancement is larger for substrate-side illumination by a factor of 2n/(n+1) despite the smaller incident electric field on the nanogap layer (Figure 2B). This factor of 2n/(n+1) is actually the same as the ratio of the magnetic field amplitude at the incident side metallic boundary, implying the role of surface current in the field enhancement phenomena. Such increase in near-field enhancement is also present in analytical calculations based on modal expansion [26, 30], as shown in Figure 2C.

For more direct confirmation of the near-field enhancement at the gap, nonlinear transmission behavior of the gap is explored under illumination of intense THz pulses with a peak field amplitude of 460 kV/cm and a pulse energy of 0.86 μJ [31, 32]. With the aid of field enhancement, the local field at the gap reaches ~10 V/nm to create tunneling current density – the amount of which is determined by the gap width, barrier height, and applied voltage. The generated free carrier density absorbs THz waves, expressing itself as an effective imaginary permittivity of the gap material, aluminum oxide [20, 21, 33]. The consequent decrease in transmission can, therefore, function as a direct probe for the local field enhancement at the metallic nanogaps [22]. In order to obtain high-field

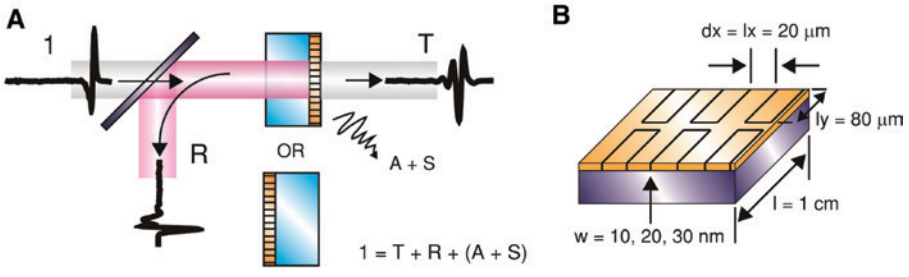

Figure 1: Experimental schematics.
(A) Transmission and reflection from nanogaps, in substrate-side or air-side incidence. A silicon beam splitter is used for normal incidence reflection measurements. (B) Geometric parameters of the rectangular ring nanogaps used in the experiment.

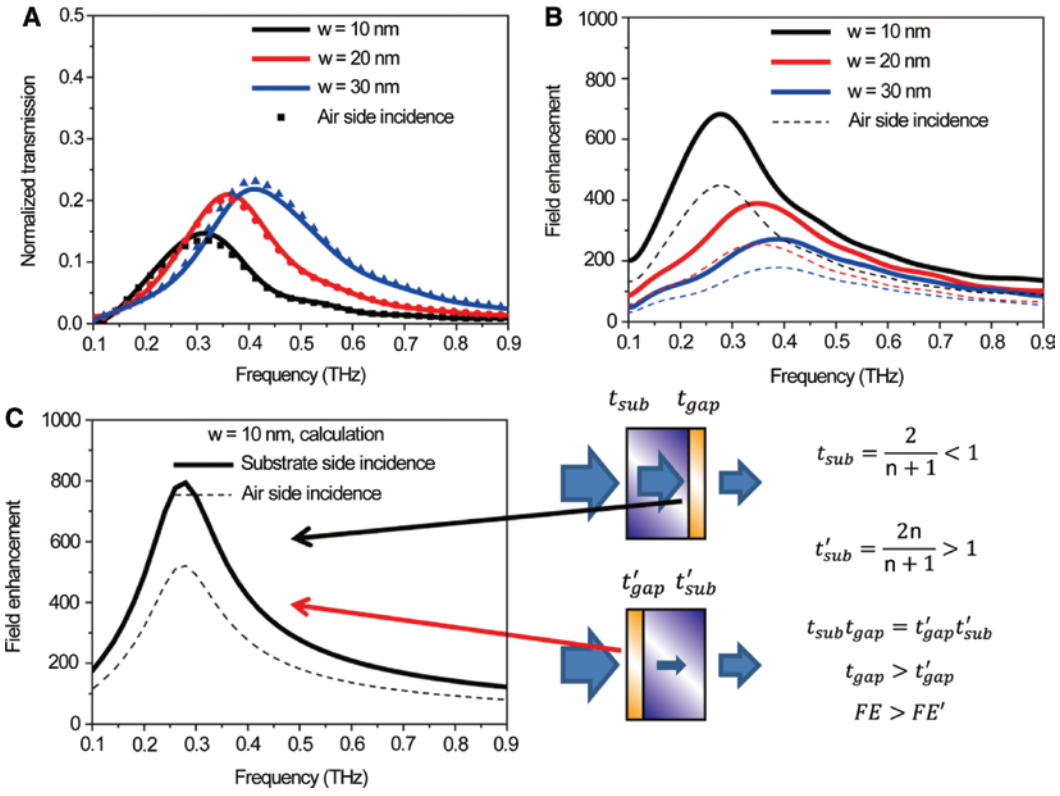

Figure 2: Transmission through the nanogaps.
(A) Normalized transmission of the nanogaps in substrate-side and air-side illumination. (B) Near-field enhancement at the gap deduced from the observed transmittance. (C) Analytically calculated field enhancement factors of 10 nm gap under substrate- or air-side incidence. The difference in the field enhancement can be understood in terms of different Fresnel coefficients for entering and exiting the substrates.

THz waves, we additionally use a regenerative amplifier and a lithium niobate crystal [34]. Figure 3 shows the power-dependent THz transmission for a 20 nm wide aluminum oxide (Al_2O_3) gap on silicon (n = 3.2), resonance-tuned at near 0.8 THz to match the THz spectrum of the lithium niobate source. Here substrate-side illumination (Figure 3A) induces larger decrease in transmitted power under the same incident electric field, confirming that the field enhancement is indeed larger than the air-side illumination case (Figure 3B). Moreover, the seemingly different transmission curves align to a single curve when the factor $2n/(n+1) = 1.52$ is considered for the field enhancement of the substrate-side incidence (Figure 3C). The substrate-induced increase in local field enhancement has been reported in metallic nanorods on top of a silicon substrate [35], but is first realized in negative slot structures with negligible direct transmission. Especially, an additional experiment with a graphene gap fabricated on quartz shows that the factor is valid regardless of the details of the nanogap structures (see Supplementary Material).

Such changes in the near field are expected to change the reflection behavior around the nanogap, because the total reflection is affected by the interference between the reflected wave at the nanogap and the direct reflected wave from the unpatterned film. Figure 4 shows the normalized reflection spectrum for the nanogaps under substrate- or air-side illumination, where the normalization is performed with the reflected signal from unpatterned Au film with the same illumination geometry. Here, the nanogap-substrate interface with higher near-field enhancement at the gap shows a larger dip in the reflection spectrum (i.e. lower reflectance) compared to the nanogap-air counterpart. The reflected power at resonance is lower than 30% for all three samples in substrate-side illumination geometry, leading to near 60% extinction overall. This seemingly abnormal extinction is also reproduced in the modal expansion analytical calculation, which expects the zeroth-order reflection from the nanogap in the form of:

$$R = 1 - \frac{4}{\pi} n_1 \beta \times \mathrm{Re}(E_{\mathrm{gap}}) + \frac{4}{\pi^2} \epsilon_1 \beta^2 \times |E_{\mathrm{gap}}|^2$$

In terms of the physics behind the phenomena, an analogy can be made with an enhanced optical absorption of a medium – in many cases solar cell – by index

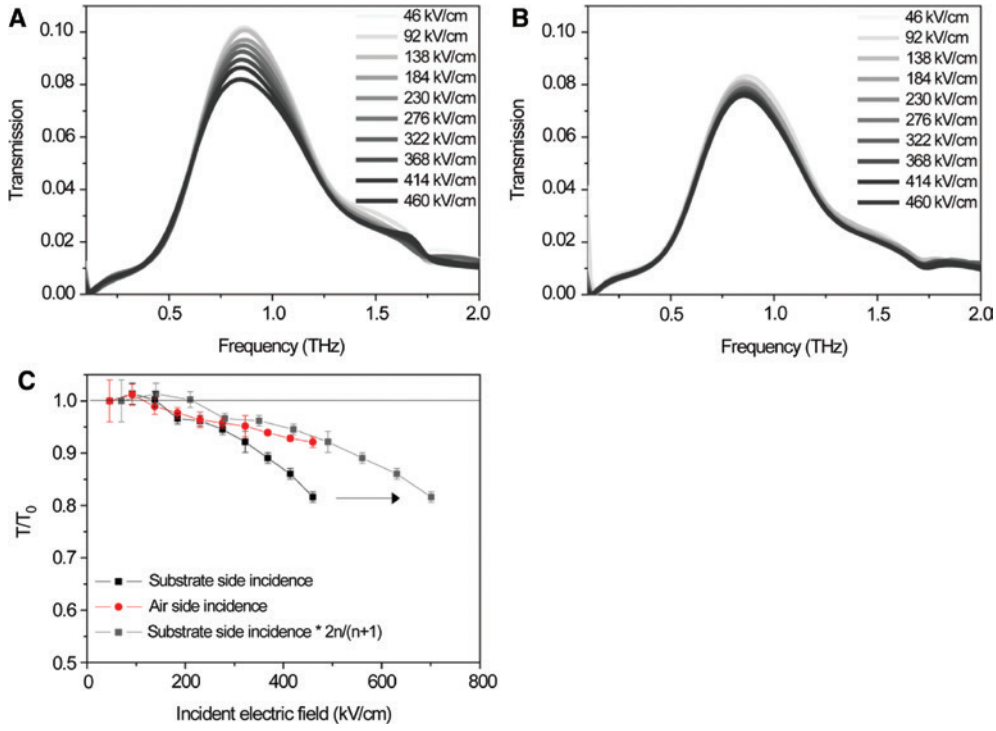

Figure 3: Power-dependent transmission of a 20 nm Al_2O_3-filled nanogap for (A) substrate-side incidences and (B) air-side incidences. (C) Different amounts of nonlinearities for the two cases under same incident electric field. Two curves fit into a single curve when the factor $2n/(n+1)$ comes into consideration for electric field amplitude in substrate-side incident case.

matching with antireflection coatings [36, 37]. When an absorbing thin film is deposited on top of a substrate, with the substrate having lower refractive index compared to that of the film but higher than that of air, the substrate can function as an index matching layer as substrate-film interface shows lower reflection coefficient than the film-air counterpart, allowing more electric field to smear into the film. This in turn leads to higher loss and lower reflection of the film, similar to what is observed in the nanogaps above. For the THz nanogaps studied in this research, the situation is similar but not the same. While there are two possible routes for the observed extinction, which are (1) Ohmic absorption of the metals and (2) scattering of nonzeroth-order diffraction from the reflection side, the absorption contribution to the total observed extinction is less than a percent due to extremely small amount of electric field penetration into the metal at THz frequencies (see Supplementary Material). What is observed here is rather analogous in part to the Mach-Zehnder modulation, where amplitudes of interfering beams are modulated via relative phases of the two input beams. At one detector the observed power decreases due to destructive interference of the out-of-phase beam, but at the other the observed power increases due to newly created path where the two beams are constructively interfering.

Such situation for the nanogaps is depicted in Figure 5, where relative phases of the electric field to the incident wave at the 10 nm gap is shown. For off-resonant frequencies the field enhancement is dominated by $-\pi/2$-out-of-phase (imaginary) component, as the surface current $\vec{K} = 2\hat{n} \times \vec{H_0}$ is in phase with the incident wave and the near field at the gap is proportional to the accumulated charge density $\sigma \propto Q = \int \vec{K} \cdot d\vec{l} dt$. At resonance an additional phase of $\pi/2$ is required in order to completely charge the gap surface, thereby leading to completely in-phase (real) component dominant feature. This means that the resonant scattering field is out of phase with the reflected electric field from metal region by a factor of π. As the near-field amplitude at the gap increases, therefore, the destructive interference of the reflected beam from metal and diffracted beam from the gaps in turn leads to a larger decrease in the zeroth-order reflection from the incident side. While there are reports on nonconservation of energy-momentum under oblique superposition of two out-of-phase waves [38], it would be more reasonable to understand the observed extinction in terms of change in the phase relation creating another path where the two beams constructively interfere, leading to energy transfer into other directions that the detection scheme cannot collect.

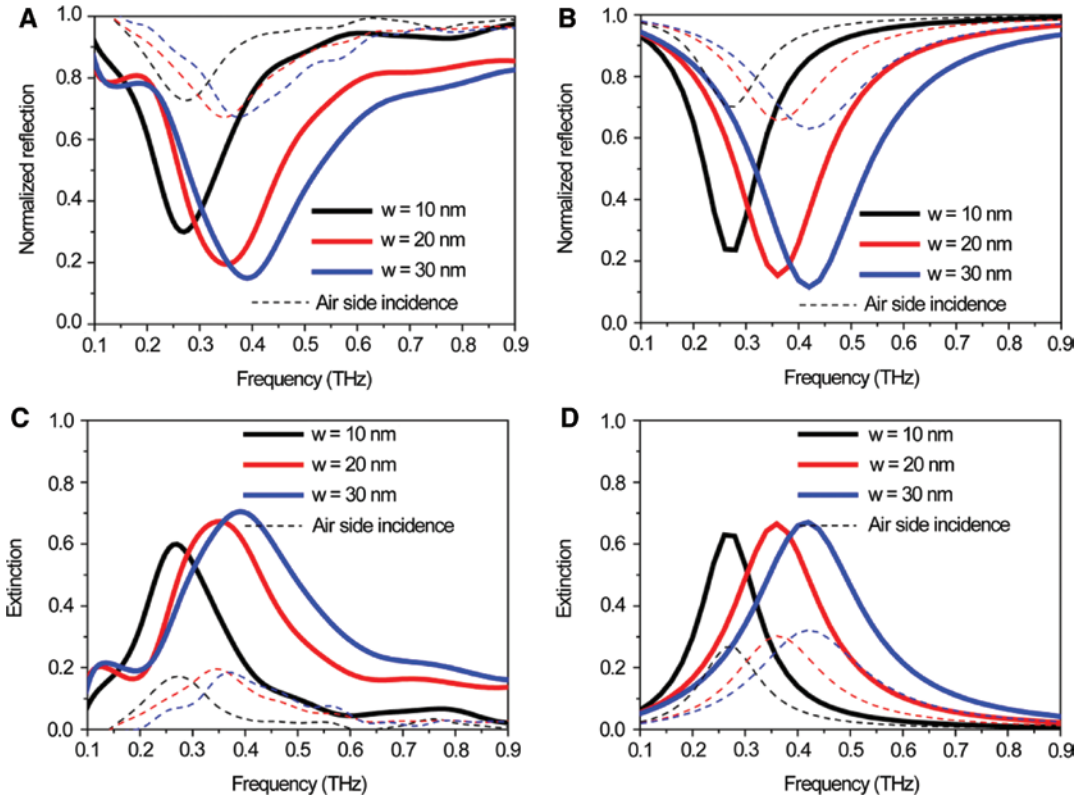

Figure 4: Reflection spectra from the nanogaps.
Substrate-side incidence induces much larger reflection dips for both (A) experiments and (B) calculations. Corresponding extinction spectra for (C) experiments and (D) calculations are also shown.

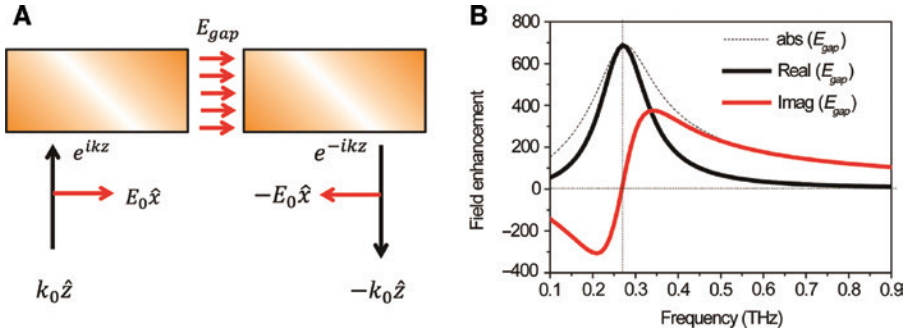

Figure 5: Phase relation between incident, reflected, and diffracted waves from the nanogap layer.
(A) Cross-sectional schematics for the relative field direction. The phase is set such that the incident wave has zero phase shift at the gap entrance. (B) Calculated complex near field at the gap, with respect to the incident wave. At resonance the near field aligns completely with the incident electric field, being out of phase with the reflected light from metal film.

This interpretation suggests an interesting possibility for the case of nanogaps coupled with an absorbing material. While a decrease in transmission is expected in the presence of the absorbing material, the reflected signal might increase because the reflection dip is proportional to the field enhancement at the gap. The total observed extinction will, therefore, not fully represent the absorption induced by the material, and might even decrease, due to a weaker backscattering from the gap. Figure 6 shows such incidence where a thin layer of water is placed on top of the nanogaps. Liquid water is a well-known THz absorber with an average absorption coefficient of 200 cm^{-1} in the frequency range of 0.1 ~ 1 THz (Figure 6D). With the near-field enhancement around the gap, as well as inside the gap, an enhancement in absorption is expected to occur for water layers on top of nanogaps. This

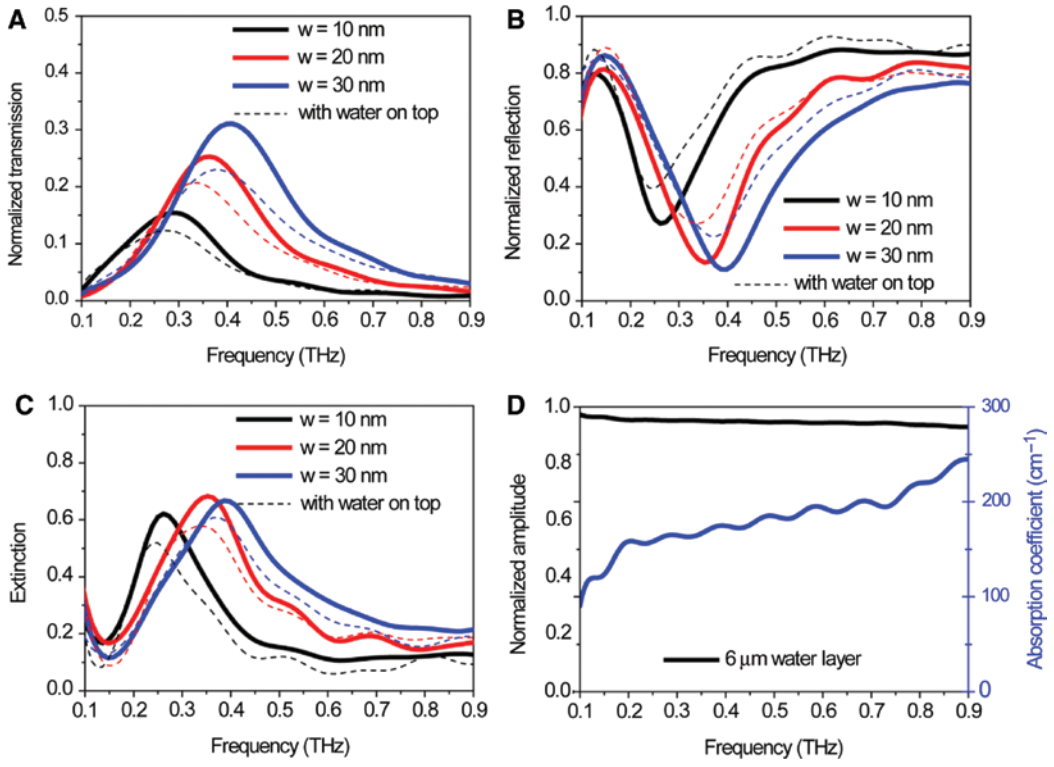

Figure 6: Substrate-side incident (A) transmission and (B) reflection data for nanogaps with and without thin water layers on top. Transmission from the nanogap-water composites are normalized with respect to that from a substrate with water layer of same thickness on top, to cancel out the effect of bulk absorption. (C) Extinction from nanogaps with and without water layer on top. (D) Transmission and absorption coefficients of 6 μm thick water layer placed on top of the nanogaps.

is clearly shown in the transmission spectra as a slight decrease in the intensity (Figure 6A). Even with the apparent decrease in total optical power, however, the reflection from the nanogap increases (Figure 6B), leading to an overall decrease in the observed extinction (Figure 6C). Such counterintuitive observation implies that reflection from the nanogaps, even with subwavelength gap width and period, is qualitatively different from that measured in a homogenous medium, and therefore does not directly represent the absorption of the structure as it does in ordinary cases.

To conclude, we experimentally and theoretically investigated the transmission and reflection from the rectangular ring nanogap structures, under different illumination geometries. Index matching effect by the substrate enables higher coupling of incident electromagnetic field to the nanogap structures, leading to higher near-field enhancement and nonlinear response at the nanogap. The near-field enhancement also induces stronger scattering from the nanogap which in turn destructively interferes with out-of-phase reflected field from the metal surface. Such interference leads to a huge decrease in zeroth order reflection, leading to an observed extinction of up to 60%. This in part resembles Mach-Zehnder modulation where relative phase relation between two beams determines the direction of power flow, leading to changes in observed power at certain direction. Such mechanism behind the anomalous reflection implies that what is not observed as either transmission or reflection cannot simply be treated as absorption, so a careful approach is required when trying to quantify nanostructure-induced absorption enhancement. This research provides a new insight into the physics behind transmission and reflection signals from the nanogap and, therefore, will be of great interest in nanogap-hybrid applications such as enhancing absorption, sensing dielectric layers, and THz nonlinear phenomena.

3 Methods

3.1 Fabrication of rectangular ring-shaped nanogaps

The nanogap samples are fabricated with atomic layer lithography technique [27]. To briefly summarize the

procedure, conventional photolithography first defines rectangle patterns, perimeters of which will later function as the nanogaps. Deposition of Au and subsequent lift-off of photoresistance lead to Au patterns with tens of micron-sized rectangular holes. Atomic layer deposition of Al_2O_3 conformally covers the whole structure with a resolution of ~1 nm. Then, directional deposition of Au fills the rectangular holes, creating vertically aligned metal-Al_2O_3-metal gap at sidewalls of the rectangular holes. Selective exfoliation of overhanging metal layer with adhesive tape reveals the gap entrance to complete the fabrication procedure.

3.2 Terahertz time-domain spectroscopy setup

For transmission and reflection measurements, a titanium-sapphire femtosecond pulse laser with 80 MHz repetition rate is used for generation of THz pulses and electro-optic sampling. A DC-biased gallium arsenide antenna is used for generating THz pulses with a center frequency at 0.4 THz. Generated THz pulses are focused onto a spot size of 3 mm with silicon lens and off-axis parabolic mirrors and is normally incident on the sample. Transmitted and reflected waves are again focused with parabolic mirrors onto a 500-micron-thick zinc telluride crystal, which incorporates electro-optic polarization change of probe beams depending on the terahertz field amplitude. The polarization change is detected with a Wollaston prism and a balanced detector, from which the field amplitude is calculated. A 2 mm-thick silicon wafer is used as a THz beam splitter for normal incidence reflection measurements. For high-power transmission measurements the basic measurement scheme is the same, with THz emission mechanism changed to tilted-front rectification from lithium niobate crystal [34]. Here the center frequency of the emitted THz wave is near 1 THz and the focus size is about 500 microns. Incident field amplitude is calculated using a THz powermeter and a known focal size, and further confirmed with the observed electro-optic signal amplitude from zinc telluride or gallium phosphide crystal.

4 Supplementary material

Discussions on lowest order mode of the rectangular ring nanogaps, details on modal expansion calculation and Kirchhoff integral formalism, additional nonlinear transmission measurements for a graphene gap, and discussions on absorption contribution to the observed extinction.

Acknowledgments: This work was supported by the National Research Foundation of Korea (NRF) grant funded by the Korean government (MSIP: NRF-2015R1A3A2031768, NRF-2016R1D1A1A02937152) (MOE: BK21 Plus Program – 21A20131111123).

References

[1] Novotny L, Van Hulst N. Antennas for light. Nat Photonics 2011;5:83–90.
[2] Kinkhabwala A, Yu ZF, Fan SH, Avlasevich Y, Mullen K, Moerner WE. Large single-molecule fluorescence enhancements produced by a bowtie nanoantenna. Nat Photonics 2009;3:654–7.
[3] Zhang WH, Huang LN, Santschi C, Martin OJF. Trapping and sensing 10 nm metal nanoparticles using plasmonic dipole antennas. Nano Lett 2010;10:1006–11.
[4] Aouani H, Rahmani M, Navarro-Cia M, Maier SA. Third-harmonic-upconversion enhancement from a single semiconductor nanoparticle coupled to a plasmonic antenna. Nat Nanotechnol 2014;9:290–4.
[5] Maier SA, Kik PG, Atwater HA, et al. Local detection of electromagnetic energy transport below the diffraction limit in metal nanoparticle plasmon waveguides. Nat Mater 2003;2:229–32.
[6] Thacker VV, Herrmann LO, Sigle DO, et al. DNA origami based assembly of gold nanoparticle dimers for surface-enhanced Raman scattering. Nat Commun 2014;5:3448.
[7] Wustholz KL, Henry AI, McMahon JM, et al. Structure-activity relationships in gold nanoparticle dimers and trimers for surface-enhanced Raman spectroscopy. J Am Chem Soc 2010;132:10903–10.
[8] Sweatlock LA, Maier SA, Atwater HA, Penninkhof JJ, Polman A. Highly confined electromagnetic fields in arrays of strongly coupled Ag nanoparticles. Phys Rev B 2005;71:235408.
[9] Dionne JA, Lezec HJ, Atwater HA. Highly confined photon transport in subwavelength metallic slot waveguides. Nano Lett 2006;6:1928–32.
[10] Jeong YG, Paul MJ, Kim SH, Yee KJ, Kim DS, Lee YS. Large enhancement of nonlinear terahertz absorption in intrinsic GaAs by plasmonic nano antennas. Appl Phys Lett 2013;103:171109.
[11] Veronis G, Fan SH. Modes of subwavelength plasmonic slot waveguides. J Lightwave Technol 2007;25:2511–21.
[12] Choi SB, Kyoung JS, Kim HS, et al. Nanopattern enabled terahertz all-optical switching on vanadium dioxide thin film. Appl Phys Lett 2011;98:071105.
[13] Park HR, Park YM, Kim HS, et al. Terahertz nanoresonators: giant field enhancement and ultrabroadband performance. Appl Phys Lett 2010;96:121106.
[14] Jeong J, Rhie J, Jeon W, Hwang CS, Kim DS. High-throughput fabrication of infinitely long 10 nm slit arrays for terahertz applications. J Infrared Millim Te 2015;36:262–8.
[15] Jo K, Dhingra DM, Odijk T, et al. A single-molecule barcoding system using nanoslits for DNA analysis. Proc Natl Acad Sci USA 2007;104:2673–8.

[16] Seo MA, Park HR, Koo SM, et al. Terahertz field enhancement by a metallic nano slit operating beyond the skin-depth limit. Nat Photonics 2009;3:152–6.
[17] BahkY-M, Han S, Rhie J, et al. Ultimate terahertz field enhancement of single nanoslits. Phys Rev B 2017;95:075424.
[18] Seo MA, Park HR, Park DJ, Kim D, Adam AJL, Planken PCM. Focusing of Terahertz waves onto micron-sized slits grown on ZnTe and gap substrates. J Kor Phys Soc 2009;55:267–70.
[19] Kyoung JS, Seo M, Park HR, Ahn KJ, Kim DS. Far field detection of terahertz near field enhancement of sub-wavelength slits using Kirchhoff integral formalism. Opt Commun 2010;283:4907–10.
[20] Bahk YM, Kang BJ, Kim YS, et al. Electromagnetic saturation of Angstrom-sized quantum barriers at terahertz frequencies. Phys Rev Lett 2015;115:125501.
[21] Kim JY, Kang BJ, Park J, et al. Terahertz quantum plasmonics of nanoslot antennas in nonlinear regime. Nano Lett 2015;15:6683–8.
[22] Kim JY, Kang BJ, Bahk YM, et al. Tunnelling current-voltage characteristics of Angstrom gaps measured with terahertz time-domain spectroscopy. Sci Rep 2016;6:29103.
[23] Lee DK, Kang JH, Lee JS, et al. Highly sensitive and selective sugar detection by terahertz nano-antennas. Sci Rep 2015;5:15459.
[24] Park HR, Ahn KJ, Han S, Bahk YM, Park N, Kim DS. Colossal absorption of molecules inside single terahertz nanoantennas. Nano Lett 2013;13:1782–6.
[25] Sharma B, Frontiera RR, Henry AI, Ringe E, Van Duyne RP. SERS: materials, applications, and the future. Mater Today 2012;15:16–25.
[26] Garcia-Vidal FJ, Moreno E, Porto JA, Martin-Moreno L. Transmission of light through a single rectangular hole. Phys Rev Lett 2005;95:103901.
[27] Chen XS, Park HR, Pelton M, et al. Atomic layer lithography of wafer-scale nanogap arrays for extreme confinement of electromagnetic waves. Nat Commun 2013;4:2361.
[28] Ordal MA, Bell RJ, Alexander RW Jr, Long LL, Querry MR. Optical properties of fourteen metals in the infrared and far infrared: Al, Co, Cu, Au, Fe, Pb, Mo, Ni, Pd, Pt, Ag, Ti, V, and W. Appl Opt 1985;24:4493.
[29] Ordal MA, Bell RJ, Alexander RW Jr, Long LL, Querry MR. Optical properties of Au, Ni, and Pb at submillimeter wavelengths. Appl Opt 1987;26:744–52.
[30] Garcia-Vidal FJ, Martin-Moreno L, Moreno E, Kumar LKS, Gordon R. Transmission of light through a single rectangular hole in a real metal. Phys Rev B 2006;74:153411.
[31] Yeh KL, Hoffmann MC, Hebling J, Nelson KA. Generation of 10 mJ ultrashort terahertz pulses by optical rectification. Appl Phys Lett 2007;90:171121.
[32] Hirori H, Doi A, Blanchard F, Tanaka K. Single-cycle terahertz pulses with amplitudes exceeding 1 MV/cm generated by optical rectification in LiNbO3. Appl Phys Lett 2011;98:091106.
[33] Esteban R, Borisov AG, Nordlander P, Aizpurua J. Bridging quantum and classical plasmonics with a quantum-corrected model. Nat Commun 2012;3:825.
[34] Sell A, Leitenstorfer A, Huber R. Phase-locked generation and field-resolved detection of widely tunable terahertz pulses with amplitudes exceeding 100 MV/cm. Opt Letts 2008;33:2767–9.
[35] Tarekegne AT, Iwaszczuk K, Zalkovskij M, Strikwerda AC, Jepsen PU. Impact ionization in high resistivity silicon induced by an intense terahertz field enhanced by an antenna array. New J Phys 2015;17:043002.
[36] Zhu J, Yu ZF, Burkhard GF, et al. Optical absorption enhancement in amorphous silicon nanowire and nanocone arrays. Nano Lett 2009;9:279–82.
[37] Munday JN, Atwater HA. Large Integrated absorption enhancement in plasmonic solar cells by combining metallic gratings and antireflection coatings. Nano Lett 2011;11:2195–201.
[38] Sze MWC, Sugon QM, McNamara DJ. Oblique superposition of two elliptically polarized lightwaves using geometric algebra: is energy-momentum conserved? J Opt Soc Am A 2010;27:2468–79.

Supplemental Material: The online version of this article offers supplementary material (https://doi.org/10.1515/nanoph-2017-0058).